Bulletin of Engineering Geology and the Environment
https://doi.org/10.1007/s10064-018-1353-z

ORIGINAL PAPER

A method for microstructure similarity clustering and feature reconstruction for weathered weak muddy intercalations

Qijun Hu[1] · Tianjun He[1] · Tao Ye[2] · Qijie Cai[3] · Songsheng He[1] · Leping He[1]

Received: 9 June 2017 / Accepted: 18 July 2018

Abstract

Weak muddy intercalations (WMI) are a type of geo-material with highly unstable mechanical properties, and thus they pose a great threat to the stability of rock slopes and in other rock engineering situations. In this paper, microstructure similarity-based clustering together with image fusion and reconstruction are used to study the microstructures of shallow weathered WMI. The study aims to obtain a reconstructed image of microstructure features that can represent a region to provide the basis for subsequent studies on WMI mechanical properties. The similarity of each microscopic WMI image is calculated using a similarity calculation model based on the microstructure parameters, and images are clustered based on their similarities. Then, image fusion technology is used to combine images in the same cluster. The results are as follows: (1) Similarity corresponding to a cumulative distribution probability of 80% is used as the clustering threshold; (2) The fused WMI microstructure image can represent the microstructure of a layer in the sample. In view of these findings, WMI microstructure clustering and feature reconstruction can provide evidence for studies on WMI lamina structures and failures involving these, which formed the basis for the assessment of the stability of slopes and other situations in which WMI are present.

Keywords Muddy weak intercalations · Microstructure · Similarity calculation model · Clustering · Image fusion

Introduction

Weak muddy intercalations (WMI) are a clay-type geo-material with poor mechanical properties in rock slopes, and thus are a key factor inducing the failure of slope especially under high rainfall conditions (Kawamura et al. 2007; Baotian Xu et al. 2013). In slopes in bedded formations, approximately 60% of WMI are mudstone-like materials that have undergone near surface weathering (Zheng 2012). The mechanical properties of WMI following weathering are closely related to the microstructure of the original mudstone (Dudoignon et al. 2004; Kawamura et al. 2007; Pusch and Weston 2003; Sivakumar et al. 2002). In fact according to the mesomechanics theories of Mishnaevsky and Schmauder (2001) and Van Mier and Van Vliet (2003), microstructure features of WMIs can be helpful in the prediction of their mechanical behavior. Once the reconstructed image is obtained, it can be used to build the mesomechanical model and investigate its mechanical behavior under external loads. However, only the microstructure of a very small area could be obtained in past studies, and there are still no effective methods to obtain microstructures that represent a region. Therefore, it is necessary to find a method to achieve this goal.

A review of previous studies indicates that past studies on WMI microstructure treated WMI as "homogeneous material" and did not consider the spatial distribution of different structures. Thus, they considered the results obtained from one sample to be representative of the type of WMI (Chen et al. 2014; Gutierrez et al. 2009; Gylland et al. 2013; Jiang et al. 2014; Kawamura et al. 2007; Tang et al. 2012). However, differences in microstructures (particle size, roundness, orientation, and fractal dimension) due to variations in weathering effects often lead to differences in these parameters (particularly cohesive strength **c** and friction angle **φ**), and, therefore, these results of previous studies have certain limitations. In this paper, we develop a methodology for obtaining microstructures that can represent a region by the use of microstructure clustering and feature reconstruction.

✉ Qijun Hu
huqijunswpu@163.com

[1] School of Civil Engineering and Architecture, Southwest Petroleum University, Chengdu 610500, China

[2] Ranken Railway Construction Group Co., Ltd, Chengdu 610046, China

[3] School of Transportation and Logistics, Southwest Jiaotong University, Chengdu 611756, China

Published online: 04 August 2018

As previously mentioned, because the conventional method does not consider the differences in the microstructures of the same type of WMI, no one has previously considered clustering the microstructures of WMI. Traditional clustering analysis is mainly used in data clustering, however, in recent years, because image-based clustering can handle the clustering of arbitrary shapes, it has attracted increasing attention. Image clustering is generally measured by similarity, so a group of images with high similarity can be assembled into the same cluster (Dhanachandra et al. 2015; Pandey and Khanna 2016; Wang et al. 2016). According to the specific conditions of the parameters involved in this paper, the clustering of WMI microstructure is based on its similarity.

After clustering, the clustered images need to be fused and reconstructed for practical applications. Current image fusion technologies can be divided into three levels: pixel-level fusion, feature-level fusion, and decision-level fusion (Gerke et al. 2015; Li et al. 2016; Lin et al. 2016). Pixel-level fusion can preserve the details of the original microstructure image to the maximum extent, and, therefore, a fused image of WMI microstructure that meets our requirements can be obtained by extracting the pixel and gray-scale information to fuse different images. Accordingly, microstructure parameters were extracted from scanned images of WMI samples and then clustered images of different regions based on their similarity were produced. Finally, images in the same cluster were fused to obtain a reconstructed microstructure image that represented the WMI in the region, in hope of providing evidence for WMI damage and a basis for slope stability analysis.

WMI microstructure quantification

To cluster WMI microstructure, the similarity between images should be calculated (Dhanachandra et al. 2015; Pandey and Khanna 2016; WANG et al. 2016), and thus the relevant parameters should be quantified. The accuracy of the parameter quantification has a certain influence on the clustering of the WMI structure. There are many parameters that reflect unit particles, among which particle size, roundness, orientation, and fractal dimension have high impacts on the mechanical properties so these are used to quantify the degree of similarity between images. This is to make sure that clustering of MWI microstructure is soundly related to its mechanical properties.

Scanning image acquisition

The microstructure of WMI within a profile varies because of differences in the degree of weathering. The transition from weathered into unweathered material was not clearly defined unless microstructural parameters are compared. In this study the WMI profile was subdivided into upper, middle, and lower layers, each about 3.3 mm thick, where the structural characteristics of the upper and lowers layers of the WMI were similar respectively to the overlying and underlying rock strata, while the middle layer was transitional between these.

An FEI Quanta 450 Environmental Scanning Microscope was employed to capture the microstructural images of MWI samples. Before this, the dried MWI sample was pasted on a sample board (the surface of which had been made electrically conductive by plating it with gold). The scanning process was performed in secondary electron (SE) model under a high vacuum.

The WMI samples of each of the layers were obtained in accordance with soil testing standards, following which six SEM images of different regions of the layer were obtained (Jiang et al. 2016; Kim et al. 2017). Considering that the near-surface structure of these samples is easily disturbed during the sampling process, as shown in Fig. 1a, the central part (10 mm) of the sample was selected as the sample for testing. Specifically, a small house-made ring (the diameter and height were 10 mm) was used to take cylindrical subsamples from the original sample (the diameter and height of which were 61.8 mm and 20 mm respectively). These testing samples were then subdivided and placed in the compartments as shown in Fig. 1b. In Fig. 1b, x-1-2 represents the scanning region index, where x is the sample number; 1 represents the first layer; and 2 represents the second scanning region in the first layer, and x-1 was an identifier for the regions in the first layer, and so on. The magnification of the SEM image has a great influence on the extraction of microscopic information. After comparing and analyzing scanning images at different magnifications, times 5000 (as shown in Fig. 1c) was found to be the most satisfactory magnification.

Image processing

A review of the literature (Cotecchia et al. 2016; Houben et al. 2014; Keller et al. 2013; Liu et al. 2011; Zheng et al. 2014) indicated that many examples of clay image processing technology are available, but histogram equalization (HE) was selected as the most appropriate for this application. Accordingly the contrast was enhanced and nonlinear median filtering with 3×3 templates was used to reduce image noise. Then a minimum-labeled watershed algorithm was used to segment the image through region recognition. Finally, the Rectangular AIO tool in Image-Pro Plus was used to determine the boundary of the viewport and to measure and count particles and pores in the binary viewport images. The quantification covered the parameters area, orientation angle, maximum diameter, fractal dimension, and perimeter. Particle size

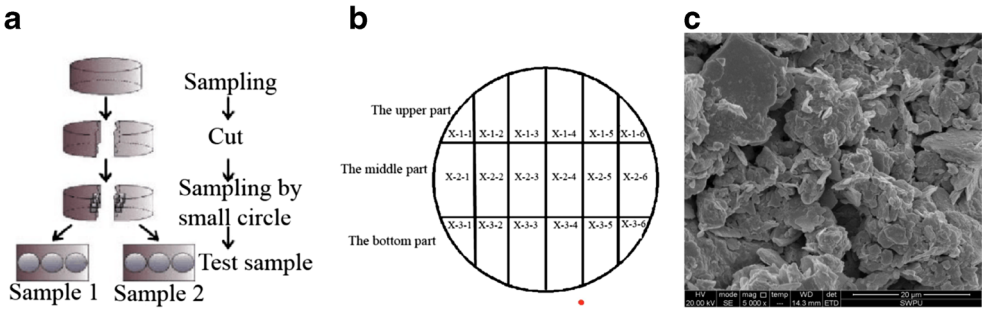

Fig. 1 **a** Division of clayey samples into subsamples; **b** partition of scanned area **c** Example of an SEM image at a magnification of ×5000

and pore diameter, particle and pore roundness, particle and pore orientation angle, and particle and pore boundary fractal dimension were thereby calculated.

Microstructure parameter similarity calculation

Similarity calculation model

In this paper, we choose the Gaussian similarity model to quantify WMI structural parameter similarity because it is suitable for calculating the similarity of data with multiple parameters and diversity. The equation is as follows (Ng et al. 2002):

$$S(M_0) = \exp\left(-\frac{d^2\left(M_0, \overline{M}\right)}{2\sigma^2}\right) \tag{1}$$

where $S(M_0)$ represents the similarity of the WMI structure image M_0; $d^2\left(M_0, \overline{M}\right)$ is the Euclidean distance between M_0 and the mean of the region in which it is located; and σ^2 represents the scale parameter for the data, that is, the dispersion (variance) of the distances between structural parameters.

The Euclidean distance of the data for a set of (M) images with n elements is defined by Deza and Deza (2009) as:

$$d(M_1, M_2) = ||M_1 - M_2||_2 = \left(\sum_{i=1}^{n} |M_{1i} - M_{2i}|^2\right)^{\frac{1}{2}} \tag{2}$$

where M_1 is a structure image; M_2 is an image constructed using parameter means; M_{1i} is the size, roundness, fractal dimension, and orientation parameter of particles and pores in M_1; and M_{2i} is the size, roundness, fractal dimension, and orientation parameter of particles and pores in M_2, where "i" is in the range 1 to 8.

The scale parameter of the structure image is the overall variance of structural parameters. Based on statistical principles (Biswas et al. 2017), the mean of the sample data is defined as follows for a given set of n samples:

$$\overline{X} = \frac{\sum_{i=1}^{n} X_i}{n} \tag{3}$$

The scale parameter (variance) of the dispersion (σ^2) of the sample data is:

$$\sigma^2 = S^2 = \frac{\sum_{i=1}^{n} \left(X_i - \overline{X}\right)^2}{n-1} \tag{4}$$

Equation (4) shows that the dispersion of structural parameters of all images can be analyzed using the mean parameters, $Mid(\gamma_1, \gamma_2, \gamma_3, \gamma_4, \varepsilon_1, \varepsilon_2, \varepsilon_3, \varepsilon_4)$, as the sample mean to calculate the scale parameter (variance σ^2) of the WMI structural parameters.

Because the range of the structural data is not within the same order of magnitude, it is meaningless to directly substitute the structural parameters into the equations for analysis. The general method is to unify the variation range of the structure parameters by normalizing each structural parameter with respect to its corresponding sample mean. That is, X_i is the ratio of each structural parameter to its corresponding sample mean, and $\overline{X}$ is 1. These ratios are then used in Eq. (4) to calculate the scale parameters: σ^2.

Similarity-based clustering

After calculating σ^2 and d^2, Eq. (1) can be used to calculate the similarity S, where the similarity between the structure images of different regions and regional means for sample #x, y are listed in Table 1 as an example.

After the similarity calculation and statistical analysis of the results, the cumulative probability map of similarity was obtained. The cumulative probability map of similarity for MWI microstructural images actually shows the functional relationships between the similarity and cumulative probability with the similarity exceeding a certain value (which is similar to the cumulative curve for grain-size distribution in soil mechanics). Because microstructures within the same layer were similar to each other, and the similarity calculated in this paper was for the same layer, most images were expected to have a similarity of 0.5 or higher. Hence, the cumulative probability with the similarity exceeding 0.5 should be much higher than 50% and drop as the similarity

Table 1 A summary table of similarity calculation results of different samples

x# Sampling area number	The numbering of scanned pictures	Similarity	y# Sampling area number	The numbering of scanned pictures	Similarity
x-1 area	x-1-1	S_{x11}	y-1 area	y-1-1	S_{y11}
	x-1-2	S_{x12}		y-1-2	S_{y12}
	x-1-3	S_{x13}		y-1-3	S_{y13}
	x-1-4	S_{x14}		y-1-4	S_{y14}
	x-1-5	S_{x15}		y-1-5	S_{y15}
	x-1-6	S_{x16}		y-1-6	S_{y16}

increases. Therefore, we assumed that the results shown in Fig. 2 would be obtained, in which the abscissa represents the similarity, and the ordinate represents percent images with equal or greater similarity.

Because differential weathering was expected to bring about a stratification of microstructures, and this study aims to cluster most (>50%) representative microstructure images of the same layer into the same cluster and then fuse them into a reconstructed image, analyses of the cumulative structural similarity map were performed. The similarity corresponding to the cumulative distribution of probability that can represent the overall situation for WMI structure image clustering was then selected. There are two extremes here: first, when the cumulative distribution probability that represents the whole situation is 100%, all the scanned images can be clustered into the same cluster, which is inconsistent with the actual situation and causes the similarity calculation to become meaningless; second, when the cumulative distribution probability that represents the overall situation is 50%, the corresponding similarity is relatively high and few images will pass the threshold, making the final fused image nonrepresentative. Therefore, the probability was set to 80%, and the similarity it corresponds to can be used as the threshold for WMI structure image clustering. Microstructural images with similarities equal to or greater than the threshold were assigned to the same cluster and considered to represent the structural features of the region. Then, the clustering results for each layer of the sample was obtained according to the similarity tables calculated.

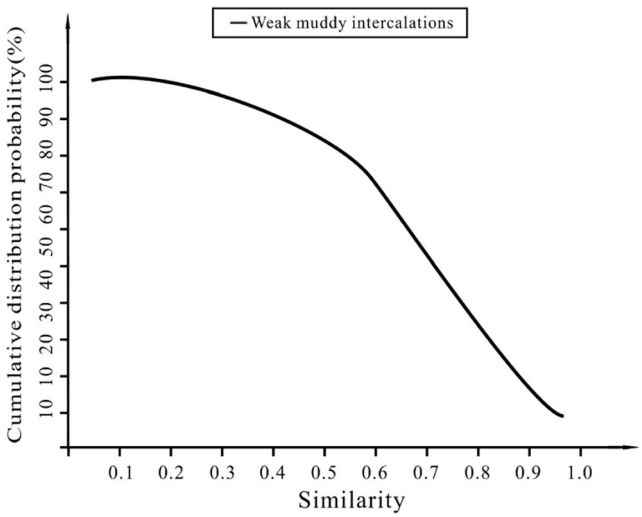

Fig. 2 Cumulative distribution probability of the similarity for one muddy intercalation

Microstructure fusion and reconstruction

To obtain the representative image of a region, WMI structure images with similar structure features were fused using an image fusion technique. To preserve the maximum amount of original structural information and represent the region at the same time, the most fundamental level of fusion, pixel-level fusion, was adopted (Ng et al. 2002). Based on the advantages and disadvantages of each fusion method, the weighted average fusion method was used to extract representative images from WMI structure images.

The mathematical expression of the weighted average fusion method is as follows:

$$F(m,n) = \omega_1 A(m,n) + \omega_2 B(m,n) \tag{5}$$

In this equation, m is the row and n is the column number of the pixel in the image; and ω_1 and ω_2 are weighting coefficients that satisfy $\omega_1 + \omega_2 = 1$. Here the images clustered into one cluster are considered to have the same representation, and thus their weighting coefficients during fusion takes the same value.

In this paper, the principle of porosity proximity-based reconstruction was adopted in which different gray thresholds were used to obtain fused images based on the grayscale histogram information for the fused image, and the fused image with the porosity closest to the original image was selected.

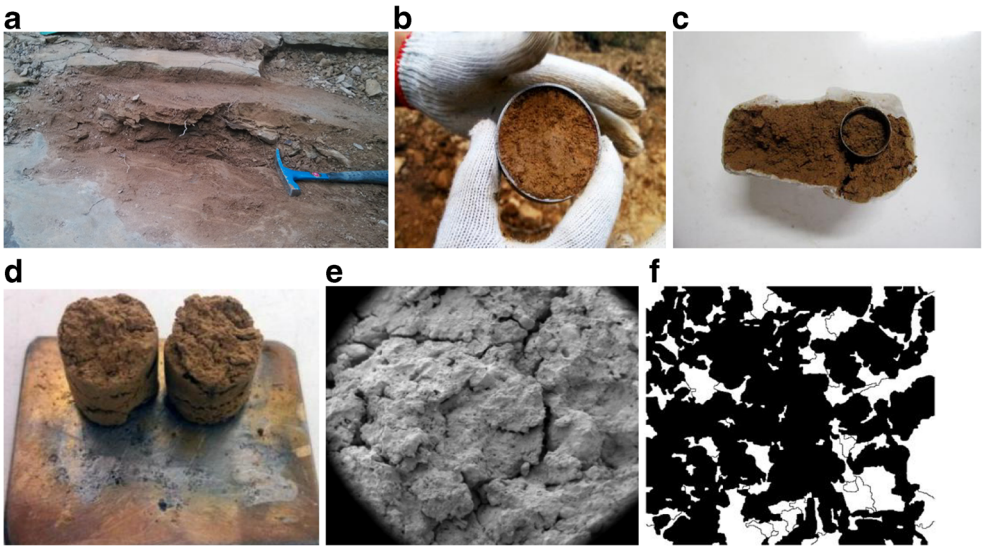

Fig. 3 **a** Sampling location, **b**–**d** sampling and subsampling operations, **e** the viewport of scanning and **f** example of processed image

Engineering application example

Sample scanning

The samples used in the study were taken from an unstable slope near Qingchuan Railway Station, on the Railway Line from Xi'an to Chengdu. The sampling procedure is illustrated in Fig. 3. The samples were taken in the field using 61.8 diameter by 200 mm high cutting ring and immediately sealed with wax. As the WMIs were thin and irregular in shape, this was to ensure that the samples were undisturbed. The samples were then divided into regions and scanned as described above — see Fig. 1, where the diameter of the small ring in Fig. 1a is 10 mm. An example of one of many processed images is shown in Fig. 3f. Image-Pro Plus was adopted to extract and analyze the structural parameters.

Clustering analysis

Sample data

At this stage, samples 1 and 2 were used as examples for similarity calculation. A partial scan of the two samples is shown in Fig. 4.

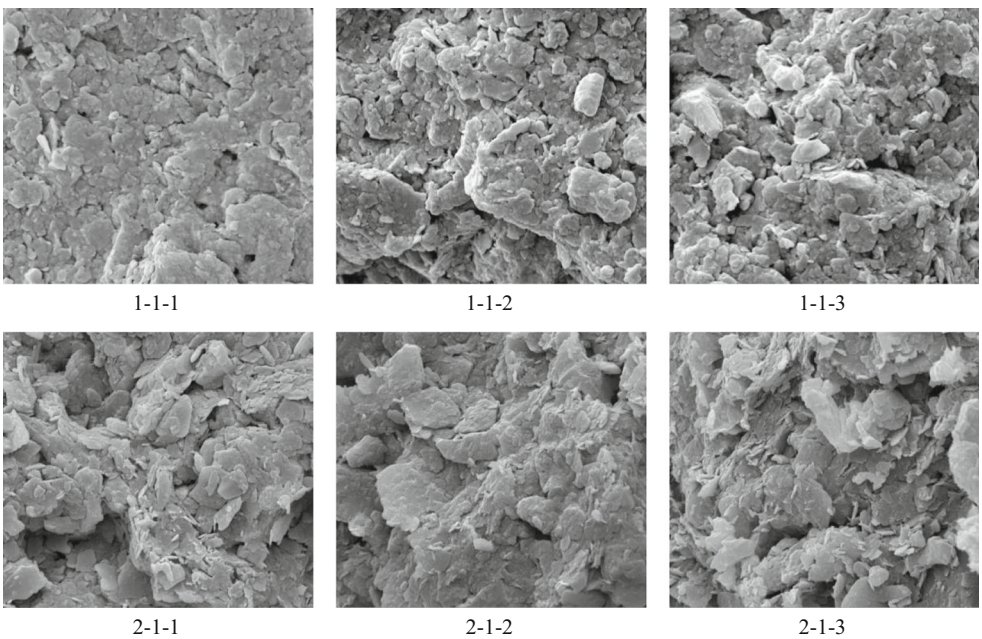

Fig. 4 SEM image of upper and middle parts of WMI

Table 2 All the parameters in the example

(a) Mean original fabric parameters of samples #1 and #2 in 1–1 and 2–1 area

	Particle parameters				Pore parameters			
Numbering	Roundness	Orientation angle/°	Particle size/μm	Fractal dimension	Roundness	Orientation angle/°	Diameter /μm	Fractal 2dimension
1–1–1	0.3218	97.0463	3.1111	1.1042	0.3316	86.5820	1.683	1.1100
1–1–2	0.3597	95.1461	3.7534	1.0967	0.5950	83.8053	1.6578	1.0441
2–1–1	0.3486	92.5271	3.1943	1.0957	0.5956	97.1015	1.7321	1.1042
2–1–2	0.3846	85.1484	3.1552	1.0964	0.6712	82.6695	1.5683	1.1012

(b) Nondimensional fabric parameters of sample #1 and #2 in 1–1 and 2–1 area

1–1–1	0.9752	1.0659	0.9692	1.0038	0.7536	0.9740	1.0788	1.0091
1–1–2	1.0900	1.0450	1.1693	0.9970	1.3523	0.9428	1.0627	0.9492
2–1–1	1.0564	1.0162	0.9951	0.9961	1.3536	1.0924	1.1103	1.0038
2–1–2	1.1655	0.9352	0.9829	0.9967	1.5255	0.9300	1.0053	1.0011

(c) Mean value of all samples

	Particle characteristic parameters				Pore characteristic parameters			
	Particle size/μm γ_1	Roundness γ_2	Orientation angle/°γ_3	Fractal dimension γ_4	Diameter /μm ε_1	Roundness ε_2	Orientation angle/°ε_3	Fractal dimension ε_4
Mean point	3.21	0.33	91.05	1.10	1.56	0.44	88.89	1.10

(d) The nondimensional fabric parameters of 1–1 regional means

	Roundness	Orientation angle	Particle size	Fractal dimension	Roundness	Orientation angle	Diameter	Fractal dimension
Means	1.0104	0.9960	1.0719	1.0057	1.0881	0.9795	1.2305	0.9966

The means for the microstructural parameters of the samples are shown in Table 2(a), the orientation angle is the angle between the major axis of the particle and the vertical direction. As mentioned in the last paragraph of section "Similarity calculation model", the dimensionless parameters given in Table 2(a) are needed to calculate the similarity.

Clustering results

The mean values obtained from the statistics for all the sample data are shown in Table 2(c) where the scale parameters were calculated according to the similarity calculation method, and the scale parameter ($\sigma_0{}^2$) for the WMI structure images took the value of 0.2531. The following example shows the calculation of the similarity between 1 and 1–1 and the mean values for layer 1.

The 1–1 regional means were calculated based on the above data, giving the results in Table 2(d):

Then, the spatial distance is (7)

$$\mathrm{d}(\mathrm{M}_1, M_2) = \sqrt{\left(\sum_{\mathrm{i}=1}^{8} (M_{1\mathrm{i}} - M_{2\mathrm{i}})\right)^2}$$

$$= \sqrt{(0.9752-1.0104)^2 + (1.0659-0.9960)^2 + (0.9692-1.0719)^2 + \cdots}$$

$$\approx 0.389928$$

Therefore, the similarity of 1–1–1 is:

$$S(M_1) = \exp\left(-\frac{d^2\left(M_1, \overline{M}\right)}{2\sigma^2}\right) = \exp\left(-\frac{0.389928^2}{2 \times 0.2531}\right) = 0.7406 \quad (6)$$

Table 3 Similarity results for different areas of the sample

1 # sample area number	The original picture number	Similarity	2 # sample area number	The original picture number	Similarity
1–1 area	1–1–1	0.7406	2–1 area	2–1–1	0.8178
	1–1–2	0.8065		2–1–2	0.7448
	1–1–3	0.5553		2–1–3	0.8695
	1–1–4	0.8892		2–1–4	0.5497
	1–1–5	0.9155		2–1–5	0.8850
	1–1–6	0.9094		2–1–6	0.8904

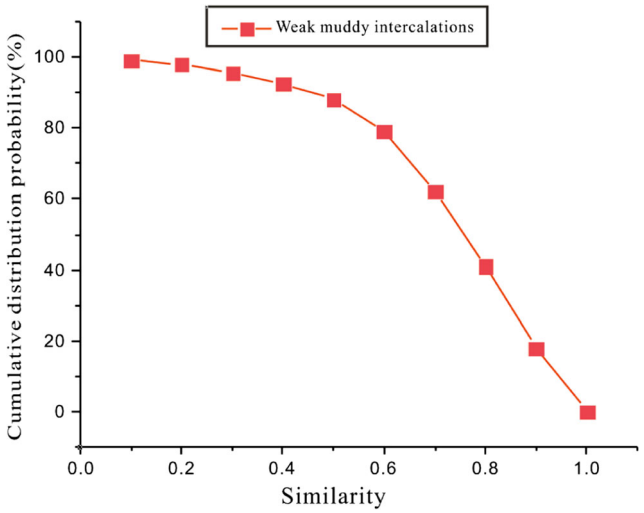

Fig. 5 WMI fabric similarity cumulative probability distribution

By calculating the similarity between structure images for different regions and the regional means, the similarity of other regions can be obtained, and the results are shown in Table 3.

The cumulative probability distribution of similarity calculated for the similarity for all the samples is shown in Fig. 5. According to the method described above, the similarity corresponding to the probability that can represent most of the samples was selected as the threshold for similarity-based clustering. The figure indicates that when the cumulative probability was 80%, the similarity was 0.6, and the clustering threshold took the value of 0.6. Table 3 shows that there were 5 images in regions 1–1 in WMI #1 and 2–1 in WMI #2 with similarity values greater than 0.6. That is, 5 images from different regions of samples #1 and #2 can represent the WMI structure of that region (the number of images is related to the number of regions), and these images can be clustered together to form a fused image. Images with similarity lower than 0.6 are considered too different from other images for the region and cannot represent the structure of the region. Therefore, they should be ignored during the clustering process.

Sample feature reconstruction

According to the structure image clustering result for region 1–1, it contained 5 representative structural images (1–1–1, 1–1–2, 1–1–4, 1–1–5, and 1–1–6). The mean porosities for each of these are compared with the porosities of the segmented reconstructed image in Table 4, and the representative image of region 1–1 shown in Fig. 6 was reconstructed based on the proposed porosity proximity-based reconstruction principle. Reconstructed feature images for regions 1–2, 1–3 were obtained using the same method, but these are not shown here.

Discussion

Representative reconstructed feature images from regions 1–1, 1–2, and 1–3 were stitched together to generate a stratified reconstructed feature image for the sample. It can be predicted that if microstructure images of the same layer from more than one sample are clustered and fused, then more of the original microstructure details can be incorporated making the final reconstructed feature image more representative of the actual microstructure.

Generally, it was assumed that the microstructure of WMI samples varied because of differences in weathering effects and the original rock lithology. However, this was overcome by considering the WMI as three sublayers, namely the upper, middle, and lower sections. SEM scanning can only capture a very limited area of WMI microstructure, making it unacceptable to select one local image to represent the whole sample. Instead, for each section, a representative reconstructed image has been obtained by combining several scanned images of the same sublayer. It should be mentioned that there may be no clear boundary between the different sublayers. Differences in the microstructure between these layers is demonstrated by the test results shown in Table 2(a). As mentioned in the introduction, the mechanical behavior of WMIs is closely related to their microstructure. Therefore, a layered structural model for WMI can be established based on the reconstructed image obtained by the method presented in this paper. This model can be used to investigate the mechanical properties of WMIs and improve the predictions of rock slope failure where WMIs have a controlling influence.

Table 4 Characteristic image porosity comparison chart Change ‘numbering’ to’ number’ and ‘Fusion’ to ‘Fused’

Sample number	01–01–01	01–01–02	01–01–04	01–01–05	01–01–06	Fused image
Porosity	0.3164	0.3277	0.3662	0.2663	0.2813	0.3504

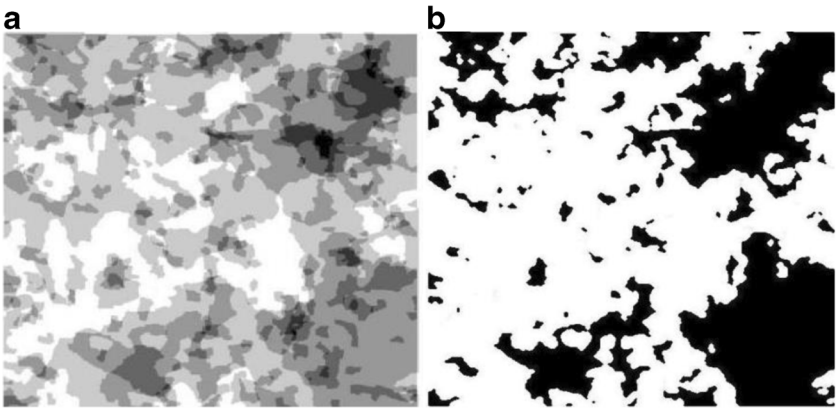

Fig. 6 The reconstructed feature images of regions 1–1. **a** Fused microstructural image of several images in the same region **b** Binaryzation result of the reconstructed image of the MWI microstructure

Conclusion

In this paper, microstructural parameters were extracted from stratified scanned images of WMI samples. Then, microstructure images of different layers were clustered and reconstructed, leading to the following conclusions:

(1) Representative WMI microstructure images were obtained using porosity proximity-based reconstruction by image fusion technology. A similarity-based WMI structure clustering method was proposed with the following general concept: structural parameter quantification → structural parameter similarity calculation→ structural parameter clustering → structural feature reconstruction.

(2) The method proposed in this paper was verified through an engineering case study. In the example the similarity corresponding to a cumulative distribution probability of 80% was used as the clustering threshold. Images with similarities above the threshold were clustered into one fused image. Representative WMI images were extracted in a stratified manner. The larger the region the similarity calculation covers, the more images will need to be formed into one cluster, thereby making the representative feature image more reliable and closer to the actual conditions.

(3) The reconstructed microstructure images can be used to establish the structural model of the WMI based on mesomechanics theory or employing numerical simulation. Then the mechanical behavior of WMI under external loads can be investigated. This is of great significance for the assessment of the stability of rock slopes and also in the design of the remediation of failed slopes. Compared with the alternative of considering the WMI as a homogeneous zone, the layered sample with representative reconstructed images can better reflect the microstructural features present in the WMI.

Acknowledgments The work was supported by the National Natural Science Foundation of China (Nos. 51574201) and the State Key Laboratory of Geo-hazard Prevention and Geo-environment Protection (Chengdu University of Technology) (SKLGP2015K006). Additional support was provided by the Scientific and Technical Youth Innovation Group (Southwest Petroleum University) (2015CXTD05).

Compliance with ethical standards

Conflict of interest The authors declare that there is no conflict of interest regarding the publication of this paper.

References

Biswas A, Rai A, Ahmad T, Sahoo PM (2017) Spatial estimation and rescaled spatial bootstrap approach for finite population. Commun Stat Theory Methods 46(1):373–388

Chen J, Dai F, Xu L, Chen S, Wang P, Long W, Shen N (2014) Properties and micro-structure of a natural slip zone in loose deposits of red beds, southwestern China. Eng Geol 183:53–64

Cotecchia F, Cafaro F, Guglielmi S (2016) Microstructural changes in clays generated by compression explored by means of SEM and image processing. Procedia Engineer 158:57–62

Deza MM, Deza E (2009) Encyclopedia of distances. Springer, Berlin, p 1–583

Dhanachandra N, Manglem K, Chanu YJ (2015) Image segmentation using K-means clustering algorithm and subtractive clustering algorithm. Procedia Comput Sci 54:764–771

Dudoignon P, Gélard D, Sammartino S (2004) Cam-clay and hydraulic conductivity diagram relations in consolidated and sheared clay-matrices. Clay Miner 39(3):267–279

Gerke KM, Karsanina MV, Mallants D (2015) Universal stochastic multiscale image fusion: an example application for shale rock. Sci Rep 5:15880

Gutierrez NHM, de Nobrega MT, Vilar OM (2009) Influence of the micro-structure in the collapse of a residual clayey tropical soil. Bull Eng Geol Environ 68(1):107–116

Gylland AS, Rueslåtten H, Jostad HP, Nordal S (2013) Microstructural observations of shear zones in sensitive clay. Eng Geol 163:75–88

Houben M, Desbois G, Urai J (2014) A comparative study of representative 2D micro-structures in shaly and sandy facies of Opalinus clay (Mont Terri, Switzerland) inferred form BIB-SEM and MIP methods. Mar Pet Geol 49:143–161

Jiang M, Zhang F, Hu H, Cui Y, Peng J (2014) Structural characterization of natural loess and remolded loess under triaxial tests. Eng Geol 181:249–260

Jiang C, Zhou X, Tao G, Chen D (2016) Experimental study on the performance and micro-structure of cementitious materials made with dune sand. Adv Mater Sci Eng. https://doi.org/10.1155/2016/2158706

Kawamura K, Ogawa Y, Oyagi N, Kitahara T, Anma R (2007) Structural and fabric analyses of basal slip zone of the Jin'nosuke-dani landslide, northern Central Japan: its application to the slip mechanism of décollement. Landslides 4(4):371–380

Keller LM, Schuetz P, Erni R, Rossell MD, Lucas F, Gasser P, Holzer L (2013) Characterization of multi-scale microstructural features in Opalinus clay. Microporous Mesoporous Mater 170:83–94

Kim SK, Kang ST, Kim JK, Jang IY (2017) Effects of particle size and cement replacement of LCD glass powder in concrete. Adv Mater Sci Eng. https://doi.org/10.1155/2017/3928047

Li H, Liu X, Yu Z, Zhang Y (2016) Performance improvement scheme of multifocus image fusion derived by difference images. Signal Process 128:474–493

Lin S-z, Wang D-j, Wang X-x, Zhu X-h (2016) Multi-band texture image fusion based on the embedded multi-scale decomposition andpossibility theory. Spectrosc Spectr Anal 36(7):2337–2343

Liu C, Shi B, Zhou J, Tang C (2011) Quantification and characterization of microporosity by image processing, geometric measurement and statistical methods: application on SEM images of clay materials. Appl Clay Sci 54(1):97–106

Mishnaevsky LL, Schmauder S (2001) Continuum mesomechanical finite element modeling in materials development: a state-of-the-art review. Appl Mech Rev 54(1):49–67

Ng AY, Jordan MI, Weiss Y (2002) On spectral clustering: analysis and an algorithm. In: Jordan MI, LeCun Y, Solla SA (eds) Advances in neural information processing systems. MIT Press, Cambridge, pp 849–856

Pandey S, Khanna P (2016) Content-based image retrieval embedded with agglomerative clustering built on information loss. Comput Electr Eng 54:506–521

Pusch R, Weston R (2003) Microstructural stability controls the hydraulic conductivity of smectitic buffer clay. Appl Clay Sci 23(1):35–41

Sivakumar V, Doran I, Graham J (2002) Particle orientation and its influence on the mechanical behaviour of isotropically consolidated reconstituted clay. Eng Geol 66(3):197–209

Tang Y-q, Zhou J, Hong J, Yang P, Wang J-x (2012) Quantitative analysis of the micro-structure of shanghai muddy clay before and after freezing. Bull Eng Geol Environ 71(2):309–316

Van Mier JGM, Van Vliet MRA (2003) Influence of microstructure of concrete on size/scale effects in tensile fracture. Eng Fract Mech 70(16):2281–2306

Wang C-l, Wang H-W, Hu B-l, Wen J, Xu J, Li X-J (2016) A novel spatial-spectral sparse representation for hyperspectral image classification based on neighborhood segmentation. Spectrosc Spectr Anal 36(9):2919–2924

Xu B, Yan C, Xu S (2013) Analysis of the bedding landslide due to the presence of the weak intercalated layer in the limestone. Environ Earth Sci 70:2817–2825

Zheng L-N (2012) Reaserch of failure mechanism and the local failure zones for consequent slope based on strain softening theory. Southwest Jiao Tong University, Chengdu

Zheng Y, Liu J, Hu Q, Cai Q (2014) Study on micro-structure of muddy intercalation using SEM method. Electron J Geotech Eng 19:9953–9963